JOURNAL OF SPACECRAFT AND ROCKETS
Vol. 32, No. 5, September–October 1995

Sloshing-Induced Moment Driven by Gravity Gradient Associated with Spacecraft Slew Motion

R. J. Hung* and H. L. Pan†
University of Alabama in Huntsville, Huntsville, Alabama 35899

The mathematical formulation of spacecraft sloshing for a partially liquid-filled cryogenic helium II in a Dewar container driven by the gravity-gradient acceleration associated with slew motion is studied. The Advanced X-Ray Astrophysics Facility—Spectroscopy spacecraft is chosen as an example in this study. Explicit mathematical expressions that manage orbital gravity-gradient acceleration associated with slew motion acting on the spacecraft fluid systems are derived. The numerical computation of sloshing reaction forces and moment fluctuations exerted on the Dewar container are investigated. This study discloses the liquid–vapor interface fluctuations modulated by sloshing dynamics the slosh reaction forces, and the moment fluctuations exerted on the spacecraft system. The relationship with the major driving force of gravity-gradient acceleration associated with slew motion on the fluid system in microgravity environment is also presented.

Nomenclature

$\boldsymbol{a}_{gg}$	= $(a_{gg,r}, a_{gg,\theta}, a_{gg,z})$, gravity gradient vector in cylindrical coordinates
$\boldsymbol{d}$	= vector (not a unit vector) from the fluid element to the spacecraft mass center
(F_x, F_y, F_z)	= fluid stress force in Cartesian coordinates
g_0	= 9.81 m/s^2, Earth gravity acceleration
h	= spacecraft orbit altitude, 650 km for AXAF
L	= height of Dewar tank, cm
(L_x, L_y, L_z)	= moment arm in Cartesian coordinates
(M_x, M_y, M_z)	= fluid stress moment in Cartesian coordinates
n	= orbit rate of spacecraft, 1.07×10^{-3} rad/s for AXAF
$\hat{\boldsymbol{n}}_\beta$	= unit vector normal to the wall
P	= thermodynamic pressure
R_c	= radius of spacecraft circular orbit, $R_E + h$, 7023 km for AXAF
(r, θ, z)	= cylindrical coordinates
$\hat{\boldsymbol{r}}_c$	= unit vector from the spacecraft mass center to the center of the Earth
R_E	= radius of the Earth, 6373 km
t	= time, s
$\hat{\boldsymbol{t}}_\alpha$	= unit vector tangential to the wall
(u, v, w)	= velocity in cylindrical coordinates (cm/s)
x, y, z	= Cartesian coordinates for fluid-dynamics computation
x'', y'', z''	= Cartesian coordinates originating at spacecraft mass center for spinning and/or slew motions
$\delta_{\alpha\beta}$	= Kronecker's delta function
ρ	= density of fluid
Π	= fluid stress
μ	= viscous coefficient of fluid
ω	= angular velocity of spacecraft spinning along the z-axis
τ	= spacecraft gravity turnaround time (s)
τ_0	= orbit period of spacecraft, 97.6 min for AXAF
ψ_E	= azimuth angle of the Earth toward the spacecraft mass center

Subscripts

c	= location at spacecraft mass center
L	= liquid
n	= components normal to the wall
t	= components tangential to the wall
V	= vapor
x, y, z	= components along the x, y, z directions
α, β	= direction of flow field

Superscripts

r–z	= components in the r–z plane
r–θ	= components in the r–θ plane

Introduction

TO carry out scientific experiments, some experimental spacecraft use cryogenic cooling for observation instruments and telescopes, for superconducting sensors for gyro readout, and to maintain a temperature near absolute zero for mechanical stability. The techniques for both cooling and control involve the use of superfluid liquid helium II. For example, both the Gravity Probe—B (GP-B) and the Advanced X-Ray Astrophysics Facility—Spectroscopy (AXAF-S) spacecraft use the cooling and boiloff from the cryogenic liquid helium Dewar as a cryogen and a propellant to maintain the cooling of instruments, attitude control, and drag-free operation of the spacecraft. The potential problems for cryogenic liquid in a Dewar container are due to sloshing-induced asymmetry in the liquid–vapor distribution and to perturbations in the liquid–vapor interface caused by a slosh-wave excitation driven by pointing control, machinery vibration, etc.

For both the GP-B and the AXAF-S spacecraft, cryogenic liquid helium II, at a temperature of 1.3 K, is used as the propellant. Because of its superfluidity, there is no temperature gradient in the liquid helium. In the absence of a temperature gradient along the surface that drives Marangoni convection, the equilibrium shape of the liquid–vapor interface is governed by a balance of capillary, centrifugal, and gravitational forces. Determination of liquid–vapor interface profiles based on computational experiments can uncover details of the flow that cannot be easily visualized or measured experimentally in a microgravity environment.

Instability of the liquid–vapor interface can be induced by the presence of longitudinal and lateral accelerations. Thus, slosh waves are excited, and produce high- and low-frequency oscillations in the liquid propellant. The sources of the residual accelerations are the Earth's gravity-gradient acceleration and jitter acceleration, including atmospheric drag on the spacecraft, compressor vibration, spacecraft attitude motions arising from machinery vibrations, thruster

Received July 29, 1994; revision received Dec. 17, 1994; accepted for publication Jan. 19, 1995.

*Professor of Mechanical and Aerospace Engineering. Associate Fellow AIAA.

†Research Engineer, Department of Mechanical and Aerospace Engineering.

firings, spacecraft slew motion, pointing control of the spacecraft, crew motion, etc. A recent study[1] suggests that the high-frequency accelerations may be unimportant in comparison with the residual motions caused by low-frequency accelerations.

Time-dependent dynamical behavior of partially liquid-filled rotating vessels in reduced gravity was simulated by numerically solving the Navier–Stokes equations subject to the appropriate initial and boundary conditions.[2–5] At the interface between the liquid and vapor fluids, both the kinematic surface boundary condition and the interface stress conditions for components tangential and normal to the interface were applied.[6–10] The initial conditions were adopted from the steady-state formulations.[11–13] Some of the steady-state formulations of interface shapes were compared with the available experiments[14] in a free-falling aircraft (KG-135). The experiments[15] showed that the classical fluid mechanics theory is applicable for cryogenic liquid helium in large containers with sufficiently large velocities.[16,17]

In the spacecraft orbit around the Earth, the azimuth angle of Earth at the spacecraft mass center varies from 0 to 360 deg about the roll axis of the spacecraft, requiring three-dimensional calculation.

As the spacecraft moves along the orbit, any fluid capable of motion relative to the spacecraft is subject to the acceleration that arises from the gravity gradients of the Earth.[18–21] The interaction between the fluid mass and the spacecraft mass due to gravity-gradient accelerations[19] is capable of the excitation of slosh waves and the disturbance of the fluid system. In this paper, we are particularly interested in the study of the fluctuations of slosh reaction forces and torques on the solid container due to the sloshing dynamics driven by gravity-gradient acceleration associated with slew motion.

Gravity-Gradient Acceleration Associated with Slew Motion

The gravity-gradient acceleration acting on each fluid element inside the on-orbit spacecraft fluid system depends upon the distance from the fluid element to the spacecraft mass center and the direction of that displacement with respect to the center of the Earth. This acceleration has to be calculated in a noninertial frame (spacecraft-bound coordinates). Thus, the coordinate system must be transformed from the ordinary inertial frame (Earth-bound coordinates) to a noninertial frame (spacecraft coordinates).

Orbit Motion of Spacecraft

As an example, for the AXAF-S spacecraft, which is an Earth satellite orbiting at 650-km altitude directly over the poles, the orbit period τ_0 can be computed from the following expression:

$$\tau_0 = 2\pi \frac{R_c^{\frac{3}{2}}}{R_E g_0^{\frac{1}{2}}} \tag{1}$$

For the AXAF-S spacecraft, the orbit period is $\tau_0 = 97.6$ min, and orbit rate is $n = 2\pi/\tau_0 = 1.07 \times 10^{-3}$ rad/s.

As the spacecraft is orbiting around the Earth, the azimuth angle of the Earth ψ_E, with respect to the spacecraft mass center, varies with respect to time. At time $t = 0$ the roll axis of the spacecraft is aligned with the radial direction from the Earth's mass center to the spacecraft mass center. It is assumed that the spacecraft roll axis turns linearly from 0 to 360 deg over the orbit period τ_0 of the spacecraft as the spacecraft orbits around the Earth. Without slew motion, the azimuth angle ψ_{E0} can be defined as

$$\psi_{E0} = (2\pi/\tau_0)t \tag{2}$$

where t is the time measured at the instant when the direction of the spacecraft roll axis is aligned with the radial direction from the spacecraft mass center to the center of the Earth.

Slew Motion of Spacecraft

In order to carry out wide-range observations, some scientific spacecraft require slew motion with respect to the spacecraft mass center. Then the azimuthal angle given in Eq. (2) is modified through the coordinate transformation of slew motion as the spacecraft orbits around the Earth.

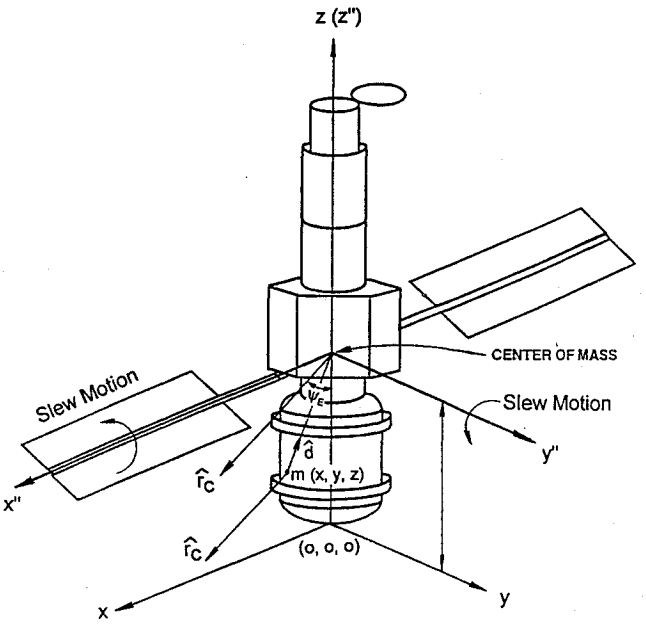

Fig. 1 AXAF-S spacecraft coordinate systems with azimuth angle ψ_E from spacecraft mass center to the center of the Earth. Coordinates (x'', y'', z'') for slew motion, and coordinates (x, y, z) for fluid-mechanics computation.

Let us assume that the slew motion starts at the mass center of the spacecraft. Let us choose Cartesian coordinates x'', y'', z'' with the z'' axis along the axis of the Dewar container (see Fig. 1). At time $t = 0$, the radius vector $\hat{r}_c$ from the spacecraft mass center to the center of the Earth lies in the x''–z'' plane of the Cartesian coordinate system (see Fig. 1). The azimuthal angle ψ_E is defined as the angle between the radial vector $\hat{r}_c$ and the z'' axis. The rotation matrices for spinning and/or slew motions along the x'', y'', and z'' axes can be expressed as

$$\begin{bmatrix} 1 & 0 & 0 \\ 0 & \cos\omega_x t & \sin\omega_x t \\ 0 & -\sin\omega_x t & \cos\omega_x t \end{bmatrix}, \quad \begin{bmatrix} \cos\omega_y t & 0 & -\sin\omega_y t \\ 0 & 1 & 0 \\ \sin\omega_y t & 0 & \cos\omega_y t \end{bmatrix}$$

$$\begin{bmatrix} \cos\omega_z t & \sin\omega_z t & 0 \\ -\sin\omega_z t & \cos\omega_z t & 0 \\ 0 & 0 & 1 \end{bmatrix}$$

respectively. The radial vector $\hat{r}_c$ in Cartesian coordinates without slew and spinning motion is (see Fig. 1)

$$\hat{r}_{c0} = [\sin\psi_{E0}, 0, -\cos\psi_{E0}] \tag{3}$$

For spinning motion along the z'' axis, slew motion along the y'' axis, and slew motion along the x'' axis, the radial vector $\hat{r}_c$ is

$$\hat{r}_{c;z,y,x} = \begin{bmatrix} 1 & 0 & 1 \\ 0 & \cos\omega_x t & \sin\omega_x t \\ 0 & -\sin\omega_x t & \cos\omega_x t \end{bmatrix} \begin{bmatrix} \cos\omega_y t & 0 & -\sin\omega_y t \\ 0 & 1 & 0 \\ \sin\omega_y t & 0 & \cos\omega_y t \end{bmatrix}$$

$$\times \begin{bmatrix} \cos\omega_z t & \sin\omega_z t & 0 \\ -\sin\omega_z t & \cos\omega_z & 0 \\ 0 & 0 & 1 \end{bmatrix} \begin{bmatrix} \sin\psi_{E0} \\ 0 \\ -\cos\psi_{E0} \end{bmatrix} \tag{4}$$

Mathematical formulations for the dynamics of spacecraft slew motion are quite general. In order to show a specific example in numerical simulation, spacecraft slew motion at 90 deg for 600 s along the y'' axis is considered in this study.

Gravity-Gradient Acceleration

The gravity-gradient acceleration acting on the fluid mass of the spacecraft can be shown to be

$$\hat{a}_{gg} = -n^2\left[3(\hat{r}_c \cdot \boldsymbol{d})\hat{r}_c - \boldsymbol{d}\right] \tag{5}$$

It is assumed that the gravity gradient exerted on the spacecraft mass center orbiting around the Earth on its specified orbit is zero. In other words, the gravity acceleration exerted on the spacecraft is nothing but the gravity-gradient acceleration defined in Eq. (5).

For the convenience of mathematical calculations along the yaw, pitch, and roll axes, let us describe all the parameters involved in Eq. (5) in terms of Cartesian coordinates. In order to match the computer simulation, the mathematical derivation is performed in the first quadrant. Figure 1 illustrates the geometrical relationship of the parameters shown in Eq. (5).

Let us consider the fluid element of interest, m, located at (r, θ, z) in cylindrical coordinates and at (x, y, z) in Cartesian coordinates. The origin of the two coordinate systems is located at the center bottom of the Dewar tank. The slew and/or spinning motions, mentioned earlier, are executed with respect to the spacecraft mass center with Cartesian coordinates (x'', y'', z''). The spacecraft mass center is located at $z = L_c$. Assume that the vector $\hat{r}_c$ lies in the x–z plane of the Cartesian coordinate system at time $t = 0$.

The radial vector $\hat{r}_c$ with the modification for slew and/or spinning motion along the x'', y'', and z'' axes has been derived in Eqs. (3) and (4). In view of the relationship between (x, y, z) and (x'', y'', z''),

$$\begin{bmatrix} x \\ y \\ z - L_c \end{bmatrix} = \begin{bmatrix} 1 & 0 & 0 \\ 0 & 1 & 0 \\ 0 & 0 & 1 \end{bmatrix} \begin{bmatrix} x'' \\ y'' \\ z'' \end{bmatrix} \tag{6}$$

The vector $\boldsymbol{d}$ in (x, y, z) coordinates becomes

$$\boldsymbol{d} = [-r\cos\theta, -r\sin\theta, -(z - L_c)] \tag{7}$$

Substituting Eqs. (4) with $\omega_x = \omega_y = 0$ and (7) into Eq. (5), the noninertial-frame expression for the gravity-gradient acceleration associated with spinning motion along the z axis becomes

$$\begin{bmatrix} a_{gg,x} \\ a_{gg,y} \\ a_{gg,z} \end{bmatrix}_{spin,z} = -n^2 \begin{bmatrix} 3[-r\sin\psi_{E0}\cos(\theta + \omega_z t) + (z - L_c)\cos\psi_{E0}]\sin\psi_{E0}\cos\omega_z t + r\cos\theta \\ -3[-r\sin\psi_{E0}\cos(\theta + \omega_z t) + (z - L_c)\cos\psi_{E0}]\sin\psi_{E0}\sin\omega_z t + r\sin\theta \\ -3[-r\sin\psi_{E0}\cos(\theta + \omega_z t) + (z - L_c)\cos\psi_{E0}]\cos\psi_{E0} + (z - L_c) \end{bmatrix} \tag{8}$$

Substituting Eqs. (4) with $\omega_x = \omega_z = 0$ and (7) into Eq. (5), the noninertial-frame expression for the gravity-gradient acceleration associated with slew motion along the y axis becomes

$$\begin{bmatrix} a_{gg,x} \\ a_{gg,y} \\ a_{gg,z} \end{bmatrix}_{slew,y} = -n^2 \begin{bmatrix} 3[-r\sin\psi\cos\theta + \cos\psi(z - L_c)]\sin\psi + r\cos\theta \\ r\sin\theta \\ -3[-r\sin\psi\cos\theta + \cos\psi(z - L_c)]\cos\psi + (z - L_c) \end{bmatrix} \tag{9}$$

where $\psi_E = \psi_{E0} + \omega_y t$.

Substituting Eqs. (4) with $\omega_y = \omega_z = 0$ and (7) into Eq. (5), the noninertial-frame expression of gravity-gradient acceleration associated with slew motion along the x axis becomes

$$\begin{bmatrix} a_{gg,x} \\ a_{gg,y} \\ a_{gg,z} \end{bmatrix}_{slew,x} = -n^2 \begin{bmatrix} 3A\sin\psi_{E0} + r\cos\theta \\ 3A\cos\psi_{E0}\sin\omega_x t + r\sin\theta \\ 3A\cos\psi_{E0}\cos\omega_x t + (z - L_c) \end{bmatrix} \tag{10}$$

where

$$A = -r\cos\theta\sin\psi_{E0} + \cos\psi_{E0}\,[r\sin\omega_x t\sin\theta + \cos\omega_x t\,(z - L_c)]$$

Thus, the gravity-gradient acceleration at (r, θ, z) can be computed from that at (x, y, z) shown in Eqs. (8–10), from the following relation:

$$\boldsymbol{a}_{gg} = \begin{bmatrix} a_{gg,r} \\ a_{gg,\theta} \\ a_{gg,z} \end{bmatrix} = \begin{bmatrix} \cos\theta & \sin\theta & 0 \\ -\sin\theta & \cos\theta & 0 \\ 0 & 0 & 1 \end{bmatrix} \begin{bmatrix} a_{gg,x} \\ a_{gg,y} \\ a_{gg,z} \end{bmatrix} \tag{11}$$

Sloshing Dynamics Driven by Gravity-Gradient Acceleration Associated with Slew Motion

The dynamical behavior of fluid elements inside the on-orbit spacecraft fluid system is strongly modified by the gravity-gradient acceleration associated with slew motion. In order to accommodate the effect of gravity-gradient acceleration, one has to consider the noninertial frame of the spacecraft-bound coordinates rather than the inertial frame used in the ordinary fluid-mechanics formulation. In this formulation, one has to explicitly consider the dynamical forces, including gravity-gradient acceleration, angular acceleration, centrifugal force, surface tension force, viscous stress forces, Coriolis forces, etc., acting on the fluid element inside the container in microgravity.[22,23]

Consider a closed circular cylinder that is partially filled with liquid helium, the ullage being helium vapor. Let us use the cylindrical coordinates (r, θ, z), with corresponding velocity components (u, v, w), and corresponding components $(a_{gg,r}, a_{gg,\theta}, a_{gg,z})$ of the gravity-gradient acceleration associated with slew motion. The typical governing equations of continuity and the full Navier–Stokes equations in noninertial-frame cylindrical coordinates, including gravity gradient and angular accelerations, centrifugal, surface tension, viscous, and Coriolis forces, etc., are adopted in this study.[22,23]

For the purpose of solving sloshing-dynamic problems of liquid propellant systems in orbital spacecraft under microgravity, one has to solve the governing noninertial-frame equations[22,23] accompanied by a set of initial and boundary conditions. A detailed illustration of the initial and boundary conditions concerning sloshing dynamics of fluid systems in microgravity is available[23,24] and is not repeated in this paper. Detailed descriptions of the computational algorithm applicable to cryogenic fluid management under microgravity have also been given.[6–10] In this paper, a full-scale AXAF-S spacecraft propellant Dewar tank with a radius of 68 cm and a height of 145 cm is used as an example in the numerical simulation. The propellant tank is 70% filled with cryogenic liquid helium, and the ullage is helium vapor. The temperature of cryogenic helium is 1.3 K, and the contact angle of the liquid on the Dewar wall is assumed to be 0 deg. The properties of liquid and vapor helium are listed in our previous publications as functions of fluid temperature.[16,17] The initial profiles of the liquid–vapor interface for the rotating Dewar are determined from computations based on algorithms developed for the steady-state formulation of microgravity fluid management.[25]

A staggered grid for the velocity components is used in this computer program. The marker-and-cell method[26] of studying fluid flow along a free surface is adopted. The finite difference method employed in this numerical study was the hybrid scheme.[27] The formulation for this method is valid for any arbitrary interface location between the grid points and is not limited to midpoint interface.[28] An

algorithm for a semi-implicit method[29] was used as the procedure for modeling the flowfield. The time step is determined automatically from the size of the grid points and the velocity of the flowfields. A detailed description of the computational algorithm applicable to microgravity fluid management has been given.[6–10] Figures 3a and 3b in the following show an example of the distribution of grid points for the Dewar tank of the AXAF-S spacecraft in the radial–axial plane and the radial–circumferential plane, respectively, in cylindrical coordinates.

Spacecraft Sloshing Dynamics Associated with Spinning and/or Slew Motions

Assuming that slew motion is along the y'' axis (see Fig. 1), the gravity-gradient acceleration associated with slew motion can be computed from the noninertial-frame expressions of Eqs. (8–11). It is assumed that the slew motion operates at 90 deg in 600 s.

In this example, spacecraft sloshing dynamics driven by gravity-gradient acceleration associated with slew motion along the y'' axis, shown in Fig. 1, has been investigated. As the orbital period of the AXAF-S spacecraft is 97.6 min and the period of 90-deg slew motion along the y'' axis is 600 s, the components of gravity-gradient acceleration along the x, y, z directions acting on the fluid mass located at $(r, \theta, z) = (12\text{ cm}, \pi/2, 3\text{ cm})$ are as shown in Fig. 2. This figure shows that the magnitude of the gravity-gradient acceleration is on the order of $10^{-7} g_0$ for the AXAL-S Dewar on its operation

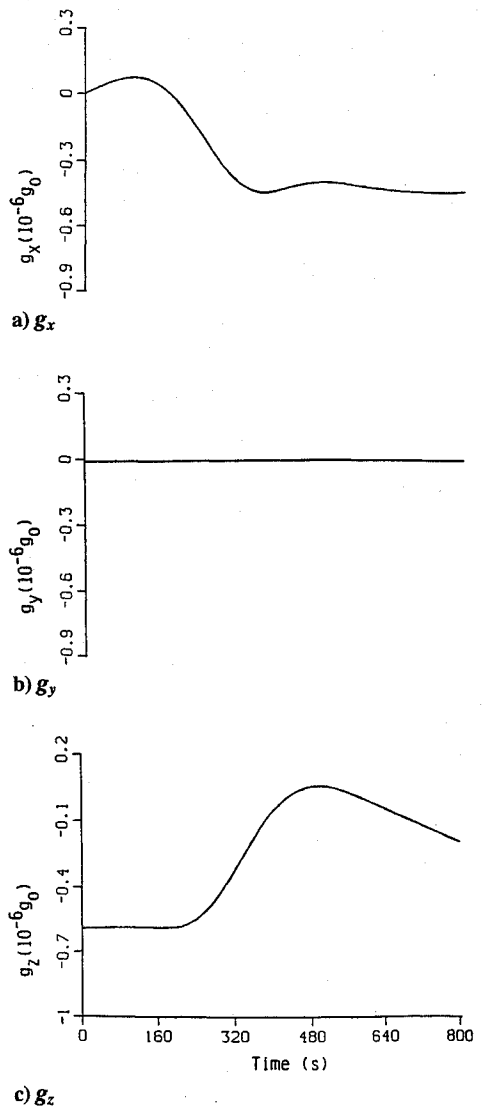

Fig. 2 Time variation of AXAF-S spacecraft gravity-gradient acceleration acting on a fluid mass located at $(r, \theta, z) = (12\text{ cm}, \pi/2, 3\text{ cm})$ for 90-deg slew motion for 600 s along the y'' axis with orbital period 97.6 min; $g_0 = 9.81\text{ m/s}^2$.

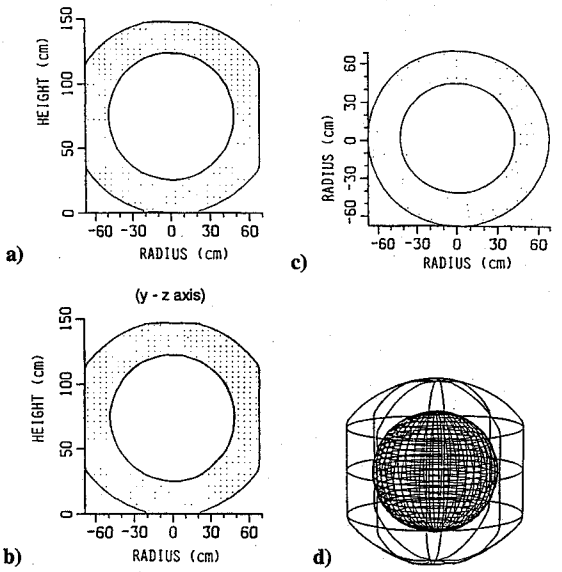

Fig. 3 Initial profiles of liquid–vapor interface for spacecraft Dewar tank under background gravity of $10^{-7} g_0$ and direction of background gravity at $\psi_E = 0$ deg: a) r–z plane at $\theta = 0$ and 180 deg (x–z axis), b) r–z plane at $\theta = 90$ and 270 deg (y–z axis), c) r–θ plane at $z = 95.9$ cm (x–y axis), and d) three-dimensional profile.

orbit. The distance from the spacecraft mass center to the bottom of the Dewar, L_c, shown in Fig. 1, is 257.8 cm.

The gravity-gradient acceleration shows the following characteristics: 1) the acceleration acting on any fluid mass inside the container decreases by two units per unit of distance measured from the spacecraft mass center to the location of the fluid mass parallel to the radial axis from the spacecraft mass center to the center of the Earth (parallel to the unit vector $\hat{r}_c$ shown in Fig. 1; and 2) the acceleration acting on the fluid mass increases by one unit per unit of the shortest distance measured from the location of the fluid mass to the radial axis along the vector from the spacecraft mass center to the center of the Earth.[19] The magnitude and the direction of gravity-gradient acceleration acting on each fluid mass are strongly dependent upon 1) how far the location of the fluid mass deviates from the spacecraft mass center measured along the axis parallel to the vector $\hat{r}_c$ and 2) how $\hat{r}_c$ varies with respect to time. It can be anticipated that the gravity-gradient acceleration acting on the fluid mass is different at different locations in the container.

The equilibrium shape of the liquid–vapor interface for a Dewar with 70% liquid filling under a residual gravity below $10^{-7} g_0$, as shown in Fig. 2, based on the computation of minimum Gibbs free energy of the bubble,[25] is a sphere. Figure 3a shows the initial shape of the interface in the r–z plane at $\theta = 0$ and 180 deg. Figure 3b shows it at $\theta = 90$ and 270 deg; Fig. 3c shows the initial profile of the liquid–vapor interface in the r–θ plane at height $z = 95.9$ cm; and Fig. 3d shows the initial profile of the three-dimensional liquid–vapor interface.

Figure 4 shows the time sequence evolution of the three-dimensional dynamical behavior of the interface oscillations driven by gravity-gradient acceleration associated with slew motion. The liquid–vapor interface profiles with the time sequences chosen in this paper are at time $t = 334$, 392, 431, 456, 487, 524, 554, 588, 600, 695, 784, and 800 s.

Comparison of Figs. 2–4 illustrates some peculiar behavior of helium temperatures below the λ point (2.17 K) in which helium demonstrates a number of remarkable properties of superfluidity[15–17] such as extremely low viscous and surface-tension coefficients in response to the disturbances driven by gravity-gradient acceleration associated with slew motion. The following results can be concluded:

1) The configuration of bubble fluctuations at time $t = 334$ s, shown in Fig. 4, indicates a near-perfect sphere, like that shown in Fig. 3, even though an extensive gravity-gradient acceleration was continuously applied to the fluid system starting at $t = 0$, shown in Fig. 2.

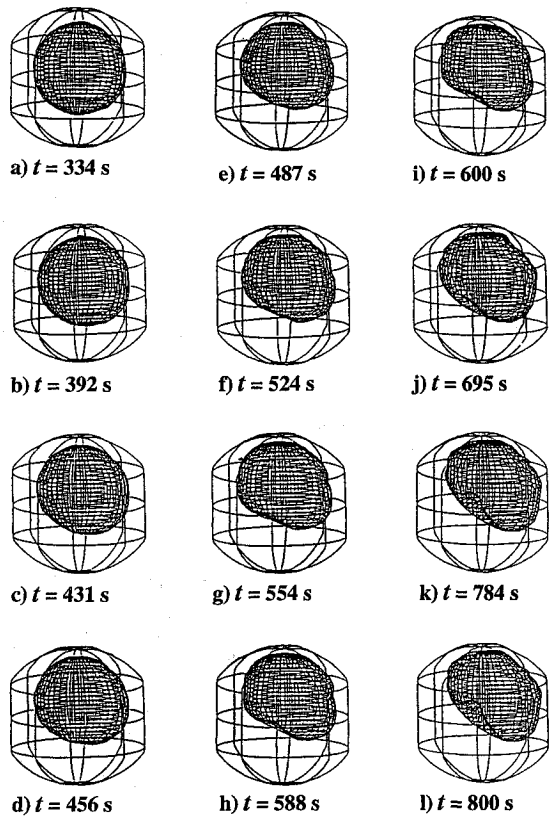

Fig. 4 Time sequence evolution of spacecraft three-dimensional liquid–vapor interface oscillations for a Dewar driven by gravity-gradient acceleration associated with slew motion along the y'' axis; liquid filling 70%.

2) The components of gravity-gradient acceleration in the x and z directions are negative, which implies that the forces are pointing toward the lower left. Thus liquid is pushed toward the lower left, while the bubble is pushed toward the upper right. These results are shown in Fig. 4.

3) The uneven and unbalanced flow velocities toward the lower left created a similar uneven and unbalanced pressure distribution pushing the bubble toward the upper right. Because of the extremely low surface tension coefficient of helium II at the liquid–vapor interface, a deformed irregular concave oscillating bubble is created.

Slosh Reaction Forces and Moment Fluctuations Due to Sloshing Dynamics

To model the slosh reaction forces and torques exerted on the Dewar by large-amplitude liquid motions, the fluid stresses are decomposed into a tangential component Π_t and a normal component Π_n relative to the walls. Their expressions are

$$\Pi_t = \mu\left(\frac{\partial u_\alpha}{\partial x_\beta} + \frac{\partial u_\beta}{\partial x_\alpha}\right)\hat{t}_\alpha \hat{n}_\beta \tag{12}$$

and

$$\Pi_n = P\delta_{\alpha\beta} - \mu\left(\frac{\partial u_\alpha}{\partial x_\beta} + \frac{\partial u_\beta}{\partial x_\alpha}\right)\hat{n}_\alpha \hat{n}_\beta \tag{13}$$

In the computation of how the slosh reaction force and torque acting on the container, the mathematical formulation in the noninertial frame (container-bound coordinates) derived earlier has to be transformed back to the inertial frame (Earth-bound coordinates).[23] Also, to accommodate the spacecraft dynamics of pitching (x), yawing (y), and rolling (z), it is convenient here to use Cartesian coordinates (x, y, z) with corresponding velocity components. For the AXAF-S spacecraft, the axis of slew motion is always fixed at the spacecraft mass center, which is located at $(x_c, y_c, z_c) = (0, 0, L_c)$, where L_c is the height of the axis of slew motion (see Fig. 1). Detailed mathematical derivation and expression of (F_x, F_y, F_z) is given in our recent work.[10]

The components of the moment can be written as the following expression[10]:

$$\begin{bmatrix} M_x \\ M_y \\ M_z \end{bmatrix} = \begin{bmatrix} L_y F_z - (L_z - L_c)F_y \\ (L_z - L_c)F_x - L_x F_z \\ L_x F_y - L_y F_x \end{bmatrix} \tag{14}$$

where L_x, L_y, and L_z denote the components of the moment arm along the x, y, and z axes, respectively. Similarly, the moment arms of the fluid stress induced by the sloshing dynamics can be computed from the following relations[10]:

$$\begin{bmatrix} L_x \\ L_y \\ L_z - L_c \end{bmatrix} = \frac{1}{F_x^2 + F_y^2 + F_z^2}\begin{bmatrix} F_y M_z - F_z M_y \\ F_z M_x - F_x M_z \\ F_x M_y - F_y M_x \end{bmatrix} \tag{15}$$

Characteristics of Slosh Reaction Force and Moment Fluctuations Exerted on the Dewar Container

Figures 5a–5c show the computed time variation of the fluctuations of slosh reaction forces exerted on the Dewar container driven by gravity-gradient acceleration associated with slew motion along

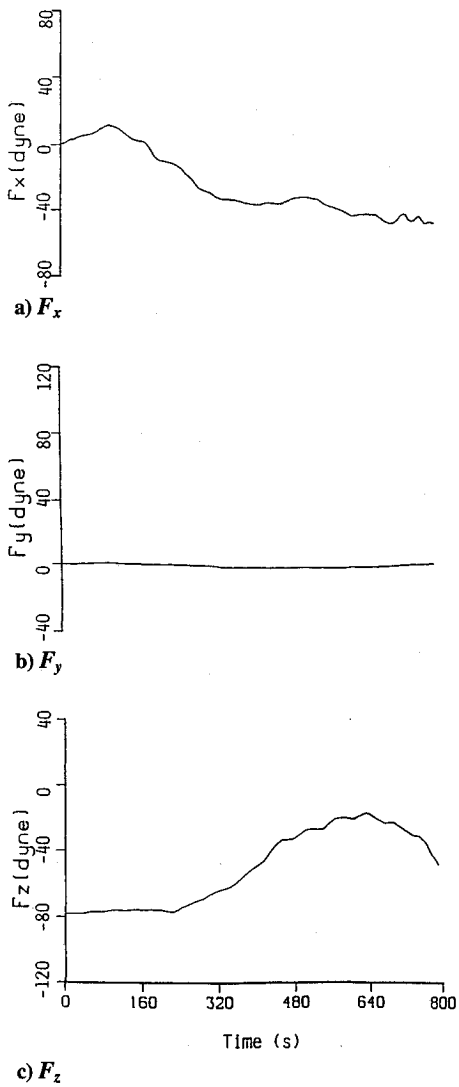

Fig. 5 Time sequence of the fluctuations of slosh reaction forces exerted on the Dewar container due to the sloshing dynamics driven by gravity-gradient acceleration associated with slew motion.

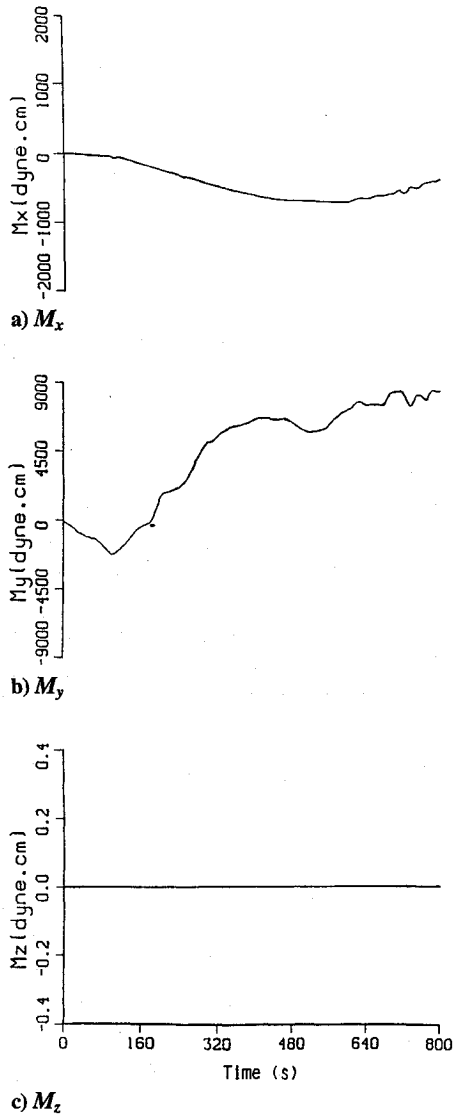

Fig. 6 Time sequence of the fluctuations of the slosh reaction moment exerted on the Dewar container due to the sloshing dynamics driven by gravity-gradient acceleration associated with slew motion along the y axis.

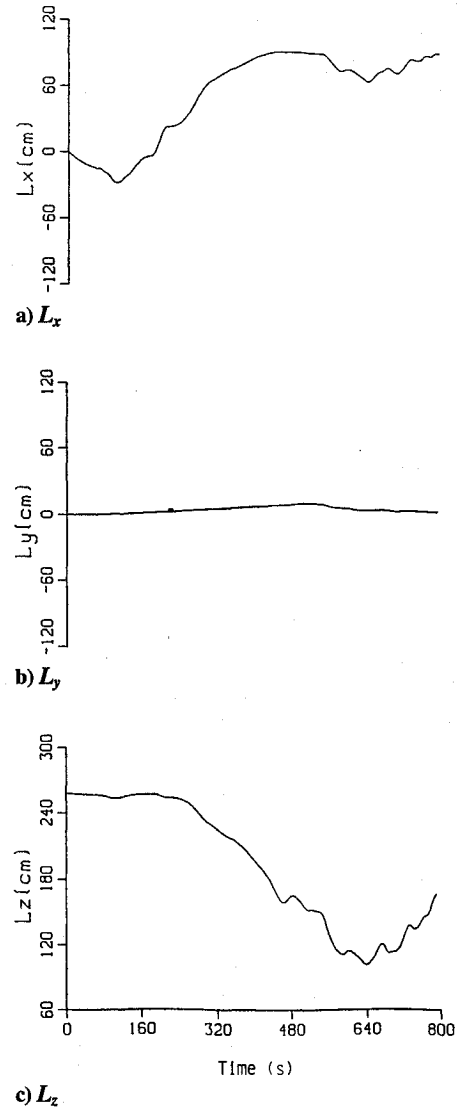

Fig. 7 Time sequence of the fluctuations of the fluid moment arm exerted on the Dewar container due to the sloshing dynamics driven by gravity-gradient acceleration associated with slew motion.

the y axis, with components along the x, y, and z axes, respectively. These figures show the following results:

1) The values of slosh reaction force fluctuations are $(\Delta F_x, \Delta F_y, \Delta F_z) = (59.2, 4.11, 61.02)$ dynes; this clearly indicates $\Delta F_z > \Delta F_x > \Delta F_y$. The maximum absolute values of slosh reaction force are $\max(|F_x|, |F_y|, |F_z|) = (47.42, 4.11, 78.68)$ dynes. This result indicates $|F_z| > |F_x| > |F_y|$.

2) The initial values of F_x and F_y are zero, while F_z starts from a nonzero value. This is due to the fact that the major driving force of gravity-gradient acceleration associated with slew motion at the beginning of slew motion is equal to zero along the x and y axes, and is nonzero along the z axis.

3) The characteristics of slosh reaction forces and their fluctuations are likely to follow the trend of the major driving force of gravity-gradient acceleration associated with slew motion in the y axis like that shown in Fig. 2. Comparison between Figs. 5 and 2 shows that the fluid system serves as a nonlinear modulator of spring mass and damper systems, amplifying and damping the forces acting on the fluid flows and then transmitting them back to the spacecraft.[8,30]

Figures 6a–6c show the variations of fluid torques exerted on the Dewar container due to sloshing dynamics driven by gravity-gradient acceleration associated with slew motion with components along the x, y, and z axes, respectively. These figures show the following results:

1) The values of the slosh reaction torque fluctuations are $(\Delta M_x, \Delta M_y, \Delta M_z) = (770.6, 10784.5, 0.0004)$ dyne · cm. The maximum absolute values of the slosh reaction torques are $\max(|M_x|, |M_y|, |M_z|) = (770.6, 8595.9, 0.0004)$ dyne · cm.

2) Because slew motion is along the y axis, the magnitudes of both ΔM_y and $|M_y|$ are maximum.

3) When slew motion is along the y axis, the value of the moment arm along the y axis is zero; also, because the y component of the major driving force of gravity-gradient acceleration associated with slew motion along the y axis is equal to zero, the magnitude $|F_y|$ is near zero. Both $|F_y|$ and L_y are small; thus $M_z = L_x F_y - L_y F_x$ is also small.

Figures 7a–7c show time fluctuations of the moment arms of slosh reaction torques exerted on the Dewar container due to sloshing dynamics driven by gravity-gradient acceleration associated with slew motion along the y axis for components along the x, y, and z axes, respectively. These figures show the following results:

1) The values of the moment arm fluctuation are $(\Delta L_x, \Delta L_y, \Delta L_z) = (119.2, 11.7, 156.1)$ cm. The maximum absolute values of the moment arm are $\max(|L_x|, |L_y|, |L_z|) = (91.3, 11.7, 257.8)$ cm. This shows $\Delta L_z > \Delta L_x > \Delta L_y$ and $|L_z| > |L_x| > |L_y|$.

2) The spacecraft slew motion is along the y axis; thus, the value of L_y is the minimum, and that of M_y is the maximum.

3) Because L_z is the function of $F_x M_y$, the value of M_y is the maximum, and that of F_x is near the maximum. Thus, the values of L_z are maximum.

4) The trend of the fluctuations of the moment arm is very much like that of the slosh reaction forces acting on the Dewar container of the spacecraft. Also, the trend of the fluctuations of the moment arm is very much like that of the major driving forces of gravity-gradient acceleration associated with slew motion along the y axis (see Figs. 7 and 2).[8,30]

Conclusions

With different scientific missions, some experimental spacecraft have to operate with various kinds of slew motion for the purpose of performing their scientific experiments. In this study, the AXAF-S spacecraft has been given as an example of a spacecraft operated with slew motion. Oscillatory motions of the liquid–vapor interface of the fluid systems can be induced by the presence of gravity-gradient acceleration associated with spacecraft slew motion. These oscillatory fluctuations originating from sloshing dynamics can cause various problems in spacecraft control systems. Sometimes, these sloshing dynamic problems can even degrade the normal operation of the spacecraft. It is virtually important to understand fully the characteristics of the spacecraft sloshing dynamics before one can assure high-quality operation of a scientific spacecraft. In this paper, we have investigated the mathematical formulation of sloshing dynamics and the associated fluctuations of slosh reaction forces and torques exerted on the container wall for a partially liquid-filled Dewar tank driven by the gravity-gradient acceleration associated with slew motion.

A numerical simulation of the slosh reaction force and torque fluctuations due to sloshing dynamics driven by gravity-gradient acceleration associated with slew motion has been conducted. The results show that there are large-amplitude fluctuations of slosh reaction forces and torques, which lead to the following conclusions:

1) For the spacecraft system as a whole, gravity-gradient acceleration associated with slew motion serves as a major driving force that acts as an input to the system, and slosh reaction forces and moments exerted on the Dewar container serve as the response activating on the spacecraft system. The conversion from input to slosh reaction system is through the nonlinear modulation of amplification and damping processes of sloshing fluid systems inside the Dewar container.

2) Characteristics of slosh reaction forces and their fluctuations exerted on the Dewar container reflect the dynamical trend of gravity-gradient acceleration associated with slew motion modulated by nonlinear sloshing dynamics. In this relationship, the fluid system serves as a nonlinear modulator with amplifications and dampings for the slosh reaction forces and torques acting on the Dewar. Eventually, through this modulation, the slosh reaction force and torque act back on the spacecraft.

3) Because the spacecraft slew motion is along the y axis, the magnitude of the fluid moments and their fluctuations along the y axis are maximum.

4) Because the spacecraft slew motion is along the y axis, the component of the fluid forces and moment arms acting on the Dewar container along the y axis is near zero.

5) Characteristics of the moment arm of sloshing dynamics acting on the Dewar container also reflect the dynamical trend of gravity-gradient acceleration associated with slew motion, which is nonlinearly modulated by the fluid systems.

The examples shown in this computation demonstrate 1) the extent to which sloshing dynamics affects the fluid forces and moments (torques) that act on the Dewar container, and 2) the relationship of fluid sloshing to the major driving force of gravity-gradient acceleration associated with slew motion. The mathematical formulation shown in this study can provide a better understanding of sloshing dynamics and its response to the orbital acceleration acting on the Dewar container, and also provide a useful tool for the development of effective control techniques to assure the high-quality operation of the spacecraft to achieve scientific missions.

Acknowledgments

The authors appreciate the support received from the National Aeronautics and Space Administration through NASA Grant NAG8-938 and also NASA Contracts NAS8-38609/Delivery Order Nos. 96 and 103. They would like to express their gratitude to Richard A. Potter of NASA Marshall Space Flight Center for stimulating discussions during the course of the present study.

References

[1]Kamotani, Y., Prasad, A., Ostrach, S., "Thermal Convection in an Enclosure Due to Vibration Aboard a Spacecraft," *AIAA Journal*, Vol. 19, No. 4, 1981, pp. 511–516.

[2]Hung, R. J., and Shyu, K. L., "Cryogenic Liquid Hydrogen Reorientation Activated by High Frequency Impulsive Reverse Gravity Acceleration of Geyser Initiation," *Microgravity Quarterly*, Vol. 1, No. 2, 1991, pp. 81–92.

[3]Hung, R. J., and Shyu, K. L., "Space-Based Cryogenic Liquid Hydrogen Reorientation Activated by Low Frequency Impulsive Reverse Gravity Thruster of Geyser Initiation," *Acta Astronautica*, Vol. 25, No. 5, 1991, pp. 709–719.

[4]Hung, R. J., and Shyu, K. L., "Constant Reverse Thrust Activated Reorientation of Liquid Hydrogen with Geyser Initiation," *Journal of Spacecraft and Rockets*, Vol. 29, No. 2, 1992, pp. 279–285.

[5]Hung, R. J., and Shyu, K. L., "Excitation of Slosh Waves Associated with Low Frequency Impulsive Reverse Gravity Acceleration of Geyser Initiation," *Acta Astronautica*, Vol. 26, No. 3, 1992, pp. 425–433.

[6]Hung, R. J., and Shyu, K. L., "Medium Frequency Impulsive Thrust Activated Liquid Hydrogen Reorientation with Geyser," *Journal of Propulsion and Power*, Vol. 8, No. 4, 1992, pp. 987–994.

[7]Hung, R. J., Lee, C. C., and Leslie, F. W., "Response of Gravity Level Fluctuations on the Gravity Probe-B Spacecraft Propellant System," *Journal of Propulsion and Power*, Vol. 7, No. 3, 1991, pp. 556–564.

[8]Hung, R. J., Lee, C. C., and Leslie, F. W., "Spacecraft Dynamical Distribution of Fluid Stresses Activated by Gravity Jitter Induced Slosh Waves," *Journal of Guidance, Control, and Dynamics*, Vol. 15, No. 4, 1992, pp. 817–824.

[9]Hung, R. J., Lee, C. C., and Leslie, F. W., "Similarity Rules in Gravity Jitter-Related Spacecraft Liquid Propellant Slosh Waves Excitation," *Journal of Fluids and Structures*, Vol. 6, No. 3, 1992, pp. 493–522.

[10]Hung, R. J., Lee, C. C., and Leslie, F. W., "Effect of the Baffle on the Spacecraft Fluid Propellant Viscous Stress and Moment Fluctuations," *Transaction of the Japan Society for Aeronautical and Space Sciences*, Vol. 35, No. 1, 1993, pp. 187–207.

[11]Hung, R. J., Tsao, Y. D., Hong, B. B., and Leslie, F. W., "Dynamical Behavior of Surface Tension on Rotating Fluids in Low and Microgravity Environments," *International Journal for Microgravity Research and Applications*, Vol. 11, No. 1, 1989, pp. 81–95.

[12]Hung, R. J., Tsao, Y. D., Hong, B. B., and Leslie, F. W., "Axisymmetric Bubble Profiles in a Slowly Rotating Helium Dewar Under Low and Microgravity Environments," *Acta Astronautica*, Vol. 19, No. 3, 1989, pp. 411–426.

[13]Hung, R. J., Tsao, Y. D., Hong, B. B., and Leslie, F. W., "Bubble Behaviors in Slowly Rotating Helium Dewar in Gravity Probe-B Spacecraft Experiment," *Journal of Spacecraft and Rockets*, Vol. 26, No. 1, 1989, pp. 167–172.

[14]Leslie, F. W., "Measurements of Rotating Bubble Shapes in a Low Gravity Environment," *Journal of Fluid Mechanics*, Vol. 161, No. 2, 1985, pp. 269–275.

[15]Mason, P., Collins, D., Petrac, D., Yang, L., Edeskuty, F., Schuch, A., and Williamson, K., "The Behavior of Superfluid Helium in Zero Gravity," *Proceedings 7th International Cryogenic Engineering Conferences* (Surrey, England, UK), Science and Technology Press, 1978.

[16]Hung, R. J., Pan, H. L., and Long, Y. T., "Peculiar Behavior of Helium II Disturbances Due to Sloshing Dynamics Driven by Jitter Accelerations Associated with Slew Motion in Microgravity," *Cryogenics*, Vol. 34, No. 8, 1994, pp. 641–648.

[17]Hung, R. J., and Long, Y. T., "Effect of Baffle on Slosh Reaction Forces in Rotating Liquid Helium Subjected to a Lateral Impulse in Microgravity," *Cryogenics* (to be published).

[18]Avduyevsky, V. S. (ed.), *Scientific Foundations of Space Manufacturing*, MIR, Moscow, USSR, 1984, p. 450.

[19]Forward, R. L., "Flattening Space-Time Near the Earth," *Phys. Rev. D*, Vol. 26, No. 3, 1982, pp. 735–744.

[20]Misner, C. W., Thorne, K. S., and Wheeler, J. A., *Gravitation*, W. H. Freeman, San Francisco, 1973, pp. 1–1279.

[21]Weinberg, S., *Gravitation and Cosmology—Principles and Applications of General Relativity*, Wiley, New York, 1972, p. 657.

[22]Hung, R. J., and Pan, H. L., "Differences in Gravity Gradient and Gravity Jitter-Excited Slosh Waves in Microgravity," *Transactions of the Japan Society for Aeronautical and Space Sciences*, Vol. 36, No. 1, 1993, pp. 153–1169.

[23]Hung, R. J., Pan, H. L., and Leslie, F. W., "Gravity Gradient or Gravity Jitter Induced Viscous Stress and Moment Fluctuations in Microgravity," *Fluid Dynamics Research*, Vol. 14, No. 1, 1994, pp. 29–51.

[24]Hung, R. J., and Pan, H. L., "Asymmetric Slosh Wave Excitation in Liquid–Vapor Interface Under Microgravity," *Acta Mechanica Sinica*, Vol. 9, No. 2, 1993, pp. 298–311.

[25]Hung, R. J., and Leslie, F. W., "Bubble Shapes in a Liquid-Filled Rotating Container Under Low Gravity," *Journal of Spacecraft and Rockets*, Vol. 25, No. 1, 1988, pp. 70–74.

[26]Harlow, F. H., and Welch, F. E., "Numerical Calculation of Time-Dependent Viscous Incompressible Flow of Fluid With Free Surface," *Physics of Fluids*, Vol. 8, No. 10, 1965, pp. 2182–2189.

[27]Spalding, D. B., "A Novel Finite-Difference Formulation for Differential Expressions Involving Both First and Second Derivatives," *International Journal of Numerical Methods in Engineering*, Vol. 4, No. 3, 1972, pp. 551–559.

[28]Patanker, S. V., and Spalding, S. D., "A Calculation Procedure for Heat, Mass, and Momentum Transfer in Three Dimensional Parabolic Flows," *International Journal of Heat and Mass Transfer*, Vol. 15, No. 8, 1972, pp. 1787–1805.

[29]Patanker, S. V., *Numerical Heat Transfer and Fluid Flow*, Hemisphere–McGraw–Hill, New York, 1980, p. 197.

[30]Hung, R. J., and Pan, H. L., "Fluid Forces Activated Spacecraft Dynamics Driven by Gravity Gradient and Jitter Accelerations in Microgravity," *Journal of Guidance, Control, and Dynamics*, Vol. 18, No. 5, 1995, pp. 1190–1196.

T. C. Lin
Associate Editor